

---

# MetaSym: A Symplectic Meta-learning Framework for Physical Intelligence

---

Pranav Vaidhyathan<sup>\*1</sup> Aristotelis Papatheodorou<sup>\*1</sup> Mark T. Mitchison<sup>2</sup> Natalia Ares<sup>1</sup> Ioannis Havoutis<sup>1</sup>

## Abstract

Scalable and generalizable physics-aware deep learning has long been considered a significant challenge with various applications across diverse domains ranging from robotics to molecular dynamics. Central to almost all physical systems are *symplectic forms*—the geometric backbone that underpins fundamental invariants like energy and momentum. In this work, we introduce a novel deep learning architecture, **MetaSym**. In particular, MetaSym combines a strong symplectic inductive bias obtained from a symplectic encoder, and an autoregressive decoder with meta-attention. This principled design ensures that core physical invariants remain intact, while allowing flexible, data-efficient adaptation to system heterogeneities. We benchmark MetaSym on highly varied datasets such as a high-dimensional spring mesh system (Otness et al., 2021), an open quantum system with dissipation and measurement backaction, and robotics-inspired quadrotor dynamics. Our results demonstrate superior performance in modeling dynamics under few-shot adaptation, outperforming state-of-the-art baselines with far larger models.

## 1. Introduction

Learning to predict the dynamics of physical systems is a fundamental challenge in scientific machine learning, with applications ranging from robotics, control, climate science, and quantum computing (Ghadami & Epureanu, 2022; Zhang et al., 2024; Alexeev et al., 2024). Traditional approaches often rely on carefully derived differential equations that embed known conservation laws and geometric properties (Papatheodorou et al., 2024) (e.g., Hamiltonian or Lagrangian mechanics). Although these classical models have been tremendously successful in capturing

fundamental physics, they can become unwieldy or intractable when confronted with complex real-world phenomena—such as high-dimensional systems, intricate interactions, or partially unknown forces—that defy simple closed-form representations. Recent progress in deep learning has opened new avenues for data-driven modeling of dynamical systems, bypassing the need for complete analytical descriptions (Carleo et al., 2019). Neural ODE frameworks (Chen et al., 2019), for instance, reinterpret dynamic evolution as a continuous function learned by a neural network, while operator-learning approaches such as Fourier Neural Operators (FNOs) (Li et al., 2021) allow for flexible mappings from initial conditions to solutions of partial differential equations. Despite these advances, deep learning approaches often face two critical challenges:

- **Preserving the underlying physical structure.** Standard networks, left unconstrained, may inadvertently violate symplectic forms, conservation of energy, or other geometric constraints intrinsic to physical dynamics (Chen et al., 2020). These violations can accumulate over time, producing qualitatively incorrect long-horizon predictions—e.g., spurious energy drift in Hamiltonian systems.
- **Generalizing across related systems.** Many real-world applications involve entire families of similar yet distinct systems (e.g., variations of a robotic manipulator differing in load mass or joint friction, or molecular systems differing in exact bonding parameters). Training an entirely separate model for each variant is both data-inefficient and computationally expensive. Without mechanisms to share knowledge, a network trained on one system will typically fail to adapt efficiently to another, even if they share most of the same physics. Bridging this sim-2-real gap is crucial for a variety of tasks such as control and real-time prediction (Bai et al., 2024).

The tension between flexibility (i.e., capacity to learn diverse dynamics) and the enforcement of physical constraints can be addressed through specialized architectures that embed geometric priors (Chen et al., 2020; Greydanus et al., 2019). Notably in the context of Hamiltonian mechanics, *symplectic networks* (SympNets) incorporate symplectic forms di-

---

<sup>\*</sup>Equal contribution <sup>1</sup>University of Oxford, United Kingdom <sup>2</sup>Trinity College Dublin, Ireland. Correspondence to: Aristotelis Papatheodorou <aristotelis@robots.ox.ac.uk>, Ioannis Havoutis <iioannis@robots.ox.ac.uk>.

rectly into their design, guaranteeing that learned transformations preserve canonical transformations (Jin et al., 2020). This preserves key invariants such as energy and momentum, mitigating error accumulation in long-horizon forecasts.

However, real-world systems also exhibit heterogeneity: varying parameters, boundary conditions, or even control signals that deviate from conservative dynamics. Thus, *meta-learning* becomes a natural extension. By training on a set of related systems, meta-learning-based methods (e.g., Model-Agnostic Meta-Learning (MAML), interpretable Meta neural Ordinary Differential Equation (iMODE) and Fast Context Adaptation Via Meta-Learning (CAVIA) (Finn et al., 2017; Li et al., 2023; Zintgraf et al., 2019b)) acquire high-level inductive biases that can be quickly adapted to novel systems using limited additional data. Consequently, when one faces a new variant of a familiar system, the network can fine-tune a handful of parameters, rather than retrain from scratch. This provides robust and scalable performance.

### 1.1. Contributions

In this work, we introduce **MetaSym**, a deep-learning framework that addresses the major challenges of data-driven modeling of physical systems, i.e., preserving underlying geometric structures to ensure physically consistent behavior over long time horizons and rapidly adapting to system variations with minimal data as mentioned in Section 1. Our contributions are listed below:

- Symplectic Encoder for Structure Preservation:** We propose a specialized neural encoder (SymplecticEncoder) built on SympNet modules. The inherent structural invariants of the SympNets provide a strong inductive bias to the SymplecticEncoder, while our bi-directional training pipeline enforces Hamiltonian consistency, obtained by the canonical transformations that pertain to different systems. Hence, the SymplecticEncoder’s output conserves key geometric invariants (e.g., energy and momentum), effectively minimizing error accumulation over long-term rollouts with minimal architecture size.
- Autoregressive Decoder with Meta-Attention for Adaptation:** To handle nonconservative forces and variations in system parameters, we introduce ActiveDecoder, a transformer-inspired decoder module equipped with a meta-attention framework. This decoder incorporates control inputs, external forces, and per-system parameters enabling flexible modeling of real-world effects beyond ideal Hamiltonian dynamics while enabling autoregressive multistep prediction during inference time.
- Meta-Learning for Multi-System Generalization:** We adopt a meta-learning motivated inner-outer training scheme wherein system-specific parameters are fine-tuned in a few gradient steps, while global parameters remain shared across systems. This yields a single framework that quickly adapts to new or modified systems with minimal additional data.

Finally, we benchmark this bespoke smaller architecture against other state-of-the-art deep learning methods, including Dissipative Hamiltonian Neural Networks (DHNNs) (Sosanya & Greydanus, 2022) and Transformers (Vaswani, 2017; Geneva & Zabarar, 2022), for modeling various physical systems in both classical and quantum regimes. These systems include a high-dimensional spring mesh system, an open quantum system whose dynamics are highly complex and counterintuitive in the classical regime, and a quadrotor with floating base dynamics. This provides evidence of far reaching implications in almost all aspects of physics modeling including challenging tasks like *real-time* quantum dynamics prediction and simulating a variety of complex dynamics that typically require complex computational methods to solve. To the best of our knowledge, MetaSym is the first bespoke physics based deep learning model, to adapt and generalize well to both classical and non-unitary quantum dynamics.

## 2. Related Work and Background

Physicists have long utilized the Lagrangian and Hamiltonian formalisms of mechanics to study the dynamics of physical systems (Kibble & Berkshire, 2004). Consider  $\mathbf{q} = (q_1, \dots, q_n)$  that represents the generalized coordinates of an  $n$ -dimensional configuration space, while  $\mathbf{p}$  represents the corresponding generalized momenta. We can describe the Hamiltonian  $H(\mathbf{q}, \mathbf{p}, t)$  as the total energy of the system. This leads to Hamilton’s equations as follows:

$$\dot{q}_i = \frac{\partial H}{\partial p_i}, \quad \dot{p}_i = -\frac{\partial H}{\partial q_i}, \quad i = 1, \dots, n. \quad (1)$$

This formalism naturally imbues the phase space  $(\mathbf{q}, \mathbf{p}) \in \mathbb{R}^{2d}$  with geometric structures that are vital to the study of these physical systems. One such structure is the symplectic form  $\omega$ , given by,

$$\omega = \sum_{i=1}^n dp_i \wedge dq_i \quad (2)$$

Concretely, a map  $\Phi_t : (\mathbf{q}(0), \mathbf{p}(0)) \mapsto (\mathbf{q}(t), \mathbf{p}(t))$  is said to be symplectic if  $\Phi_t^* \omega = \omega$ . This implies that the flow in the phase space preserves volume and the fundamental two-form  $\omega$  (Royer, 1991).

Inspired by such geometric formulations of mechanics, recent work such as Hamiltonian Neural Networks (HNNs) and Lagrangian Neural Networks (LNNs) have sought to embed physical priors into deep learning architectures (Greydanus et al., 2019; Cranmer et al., 2020). In particular, SympNets have emerged as structure-preserving neural architectures designed specifically for learning Hamiltonian systems, ensuring that their learned maps are intrinsically symplectic. They introduce modules that come in three variants: *linear* ( $\ell_{\text{up}}, \ell_{\text{low}}$ ), *activation* ( $N_{\text{up}}, N_{\text{low}}$ ) and *gradient* ( $G_{\text{up}}, G_{\text{low}}$ ). These modules decompose symplectic flows into compositions of “unit triangular” symplectic transformations. Based on these modules, these authors propose two architectures, LA-SympNets that are compositions of *linear* and *activation* modules and G-Sympnets that based on *gradient* modules exclusively. These architectures admit universal approximation theorems and crucially, this construction does not require solving ODEs or differentiating a candidate Hamiltonian during training and inference times, which often leads to more efficient optimization compared to other architectures such as HNNs or LNNs. The collection of all SympNets forms a group under composition, ensuring that every learned map is invertible with a closed-form inverse. However, due to the fundamental nature of Hamiltonian systems and symplectic forms, SympNets and similar architectures fail to generalize to dissipative systems where the symplectic structure is no longer preserved (Chen et al., 2020; Cranmer et al., 2020; Jin et al., 2020). While there have been attempts to reconcile dissipative dynamics and control inputs to model realistic physical systems by preserving the symplectic framework, such as the Dissipative SymODEN (Zhong et al., 2020; 2024), they often suffer from the lack of generalization to different systems (Okamoto & Kojima, 2024).

Generalization between different but related physical systems is also vital for deep learning methods to excel at physics modeling. Meta-learning serves as the natural avenue for exploring such strategies. Building on a series of meta-learning strategies (Finn et al., 2017; Rajeswaran et al., 2019; Zintgraf et al., 2019a; Nichol, 2018), the iMODE framework represents a notable advancement in applying deep learning to families of dynamical systems. iMODE integrates multiple new components specifically tailored to continuous-time dynamics by parameterizing a continuous-time flow  $\dot{\mathbf{x}}(t) = \mathbf{f}_{\theta}(\mathbf{x}(t), t)$  through a neural network similar to that of Neural ODEs (NODEs). When combined with MAML, iMODE introduces explicit *adaptation parameters* that act as a latent space embedding for system-specific characteristics. In this setup, one set of parameters captures the universal dynamics shared across all systems in a family, while another set encodes the idiosyncratic physical parameters that differentiate one system instance from another. However, certain drawbacks still persist. Apart

from the lack of physics priors, these existing meta-learning approaches such as iMODE suffer from a lack of scalability (Choe et al., 2023).

### 3. Methods

In this section, we detail our pipeline for learning, adapting, and predicting the dynamics of physical systems using MetaSym, our structure-preserving neural architecture and meta-learning framework. We describe both the high-level design of our *encoder–decoder* model and the specialized training procedures implemented via *meta-learning*. Figure 1 represents the overview of the architecture.

#### 3.1. SymplecticEncoder: Structure Preservation

To ensure that predictions preserve fundamental geometric invariants, the encoder module is implemented as a SymplecticEncoder. Internally, it uses a *symplectic neural network* (e.g., LASympNet (Jin et al., 2020)) consisting of sub-layers that update position  $\mathbf{q}_t^{(i)}$  and momentum  $\mathbf{p}_t^{(i)}$  for systems  $i = 1, \dots, n$  in a manner designed to approximate Hamiltonian flows and preserve symplecticity. Specifically, each sub-layer either performs an “up” or “low” transformation,

$$\begin{aligned} \text{(Up)} \quad & \mathbf{q}_t^{(i)} \leftarrow \mathbf{q}_t^{(i)} \alpha(\mathbf{p}_t^{(i)}) \Delta t, \quad \mathbf{p}_t^{(i)} \leftarrow \mathbf{p}_t^{(i)}, \\ \text{(Low)} \quad & \mathbf{q}_t^{(i)} \leftarrow \mathbf{q}_t^{(i)}, \quad \mathbf{p}_t^{(i)} \leftarrow \mathbf{p}_t^{(i)} + \beta(\mathbf{q}_t^{(i)}) \Delta t. \end{aligned} \quad (3)$$

Here,  $\alpha$  and  $\beta$  can be *linear*, *activation*-based, or *gradient*-based modules, ensuring we remain in the class of canonical (i.e., symplectic) maps. By stacking multiple up/low blocks, we achieve a deep network  $\Phi_{\theta} : (\mathbf{q}_t^{(i)}, \mathbf{p}_t^{(i)}, \Delta t) \mapsto (\mathbf{q}_{t+1}^{(i)}, \mathbf{p}_{t+1}^{(i)})$ .

A pivotal feature of Hamiltonian dynamics is *time reversibility*: if we integrate the system forward from  $(\mathbf{q}_t^{(i)}, \mathbf{p}_t^{(i)})$  to  $(\mathbf{q}_{t+1}^{(i)}, \mathbf{p}_{t+1}^{(i)})$  over time  $\Delta t$ , then integrating backwards over  $-\Delta t$  should return the system exactly to  $(\mathbf{q}_t^{(i)}, \mathbf{p}_t^{(i)})$ . This property lies at the heart of many physical invariants (energy, momentum, etc.) and is crucial for long-horizon stability.

To replicate this in the neural network, each forward pass provides the update for the forward and inverse network, where the forward network  $\Phi_{\theta_{SE}}$  is characterized as:

$$\Phi_{\theta_{SE}}(\mathbf{q}_t^{(i)}, \mathbf{p}_t^{(i)}, \Delta t) = [\mathbf{q}_{t+1}^{(i)}, \mathbf{p}_{t+1}^{(i)}], \quad (4)$$

and the inverse network  $\Phi_{\theta_{SE}}^{-1}$  acts as not merely the computationally reversed pass of  $\Phi_{\theta_{SE}}$ . It also switches the sign of  $\Delta t$  (i.e., steps “backwards in time”). From a physical standpoint, preserving both a forward and inverse map enforces the time-reversal symmetry characterizing Hamiltonian flows. We *train both directions* simultane-

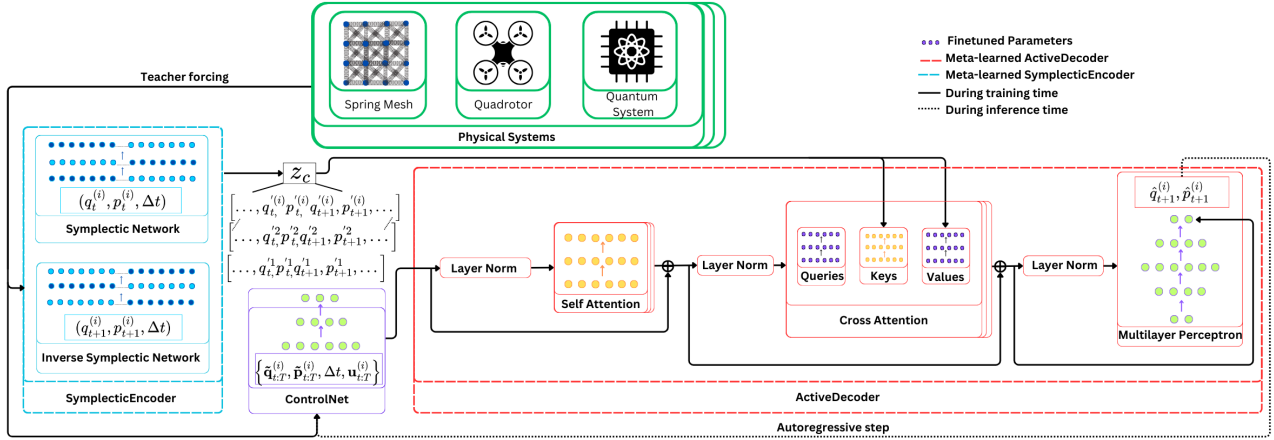


Figure 1. Schematic representation of the **MetaSym** architecture. The conservative dynamics obtained from a physical system acts as the input to the SymplecticEncoder (blue-dashed box). This module consists of the symplectic network and its inverse, represented by the alternating light blue and dark blue dots. The forward network receives  $(\mathbf{q}_t^{(i)}, \mathbf{p}_t^{(i)}, \Delta t)$  that represents the position and momentum measurements at time  $t$  for a given system  $i$  during training, while the inverse network receives the position and momentum data from the future time step  $(\mathbf{q}_{t+1}^{(i)}, \mathbf{p}_{t+1}^{(i)}, \Delta t)$ . The SymplecticEncoder outputs the latent space  $\mathbf{z}_c$ . This process can be repeated for different systems. The sequence of the non-conservative canonical coordinates and control signals,  $\{\tilde{\mathbf{q}}_{t:T}^{(i)}, \tilde{\mathbf{p}}_{t:T}^{(i)}, \Delta t, \mathbf{u}_{t:T}^{(i)}\}$ , act as inputs to the ControlNet (purple box) whose output is supplied to the ActiveDecoder (red dashed box). The ActiveDecoder consists of a layer normalization followed by a self attention layer that is then followed by layer normalization again. This is then provided to the cross attention layer which consists of keys, queries and values. The queries and values are finetuned based on a meta-update. This is finally followed by layer normalization and a multilayered perceptron (MLP) that outputs the position and momentum for the next time  $(\hat{\mathbf{q}}_{t+1}^{(i)}, \hat{\mathbf{p}}_{t+1}^{(i)})$ . During training, we provide the ground truth sequence following a teacher-forcing paradigm (black arrow). During test time, we use the network’s output for autoregressive prediction (black dotted line).

ously—minimizing reconstruction errors for forward evolution and inverse evolution. As a result, the network is less susceptible to artificial energy drift and can better maintain conservation laws over extended forecasts. The learned symplectic map remains bijective, preserving volumes in phase space and the symplectic 2-form. Moreover, we can train both passes to minimize reconstruction errors in forward and backward directions, thereby further regularizing the network to approximate canonical transformations faithfully. This invertible design also allows consistent backward integration without introducing extraneous numerical artifacts.

During training the encoder is provided with a sequence of phase-space points and encodes them onto a conservative latent space  $\mathbf{z}_c = [\mathbf{q}_{\text{enc}}, \mathbf{p}_{\text{enc}}] \in \mathbb{R}^{2d \times T}$  that is ultimately used by the ActiveDecoder as its memory sequence.

Additionally, to ensure that our encoder can generalize quickly across multiple related but distinct physical systems, we adopt a MAML-style (Finn et al., 2017) framework. For each system  $i$  in a mini-batch, we split its trajectory into  $\mathcal{I}_{\text{adapt}}$  and  $\mathcal{I}_{\text{meta}}$  sets. During the fast adaptation loop, we optimize the parameters of the encoder  $\theta_{SE}$  only on  $\mathcal{I}_{\text{adapt}}$ , by minimizing the mean-squared error between its forward predictions and the ground-truth labels. This process simu-

lates “specializing” the encoder to system  $i$ ’s local dynamics using a simple loss function that avoids gradient-terms that may destabilize the subsequent meta-update of  $\theta_{SE}$ . For the outer loop, we perform a forward and an inverse pass of the SymplecticEncoder and subsequently we minimize a combined loss represented as,

$$\mathcal{L}_{\text{meta}} = \frac{1}{\mathcal{T}_{\text{meta}} N_{\text{batch}}} \sum_{\substack{t \in \mathcal{I}_{\text{meta}} \\ i \in N_{\text{batch}}}} \left\| \Phi_{\theta_{SE}}(\mathbf{q}_t^{(i)}, \mathbf{p}_t^{(i)}; \theta_{SE}^{*(i)}) - \Phi_{\theta_{SE}}^{-1}(\mathbf{q}_{t+1}^{(i)}, \mathbf{p}_{t+1}^{(i)}; \theta_{SE}^{*(i)}) - [\mathbf{q}_{t+1}^{(i)} - \mathbf{q}_t^{(i)}, \mathbf{p}_{t+1}^{(i)} - \mathbf{p}_t^{(i)}] \right\|^2, \quad (5)$$

using the adapted parameters  $\theta_{SE}^*$ , this loss measures how well the optimal adapted parameters  $\theta_{SE}^*$  generalize beyond the adaptation subset. We accumulate gradients *with respect to*  $\theta_{SE}$  and sum across multiple batches to obtain a single update step.

### 3.2. ActiveDecoder: Autoregressive Decoder

As mentioned in Section 1.1, we train an autoregressive decoder to model non conservative and realistic forces such friction, or air resistance, that break pure Hamiltonian sym-

metries. Unlike the SymplecticEncoder, which strictly enforces canonical updates, the ActiveDecoder can incorporate these extraneous phenomena. While the former is trained in isolation, we freeze its parameters during the decoder’s training.

We define  $\hat{\mathbf{q}}_t^{(i)}$  and  $\hat{\mathbf{p}}_t^{(i)}$  as the dissipative canonical coordinates, of a system  $i$ . An input consisting of  $\{\tilde{\mathbf{q}}_t^{(i)}, \tilde{\mathbf{p}}_t^{(i)}, \Delta t, \mathbf{u}_t^{(i)}\} \in \mathbb{R}^{(2d+m+1)}$  is provided to a linear projection, where  $\mathbf{u}_t^{(i)} \in \mathbb{R}^m$  represents the control input driving the system at time  $t$ . This linear layer which we call “ControlNet”, serves to map the input to a latent vector  $\mathbf{z}_d \in \mathbb{R}^{2d}$  representing the non-conservative part of the system’s dynamics. We then apply a masked multi-head self-attention over the sequence  $\{\mathbf{z}_d\}$  for autoregressive decoding. The masking allows us to model the causal dependencies of the decoder’s input sequence.

Next, we apply a cross-attention mechanism, augmented with a specialized *meta-attention* design. To achieve multi-system generalization and fast adaptation, we use a meta-learning setup akin to a *bi-level* optimization inspired by recent progress (Li et al., 2025). Specifically, we separate the ActiveDecoder’s parameters into: global parameters,  $\theta_{AD}$ , that remain *shared* across all systems, and local parameters,  $\zeta_i$ , that can be interpreted as system specific parameters. Specifically in the meta-attention:

- *Key parameters* remain global and are updated in the outer loop, common to all systems.
- *Query/Value parameters* are re-initialized for each system and fine-tuned with a few iterations in the inner loop, allowing the decoder to discover per-system or per-task representations.

For each system  $i$ , we split the time-sequenced data,  $\{\tilde{\mathbf{q}}_t^{(i)}, \tilde{\mathbf{p}}_t^{(i)}, \mathbf{u}_t^{(i)}\}$  into an *adaptation* set,  $\mathcal{I}_{adapt}$ , and a *meta* set,  $\mathcal{I}_{meta}$ . During the *inner loop* of the bi-level optimization, we hold  $\theta_{AD}$  fixed and fine-tune  $\zeta_i$  by performing a few steps of gradient descent. Each step iterates over  $\mathcal{I}_{adapt}$  feeding the ActiveDecoder ( $\Phi_{AD}$ ) with ground-truth  $(\mathbf{q}_t^{(i)}, \mathbf{p}_t^{(i)})$  and control  $\mathbf{u}_t^{(i)}$ , and minimizing an inner MSE loss:

$$\mathcal{L}_{inner}^{(i)} = \frac{1}{\mathcal{I}_{adapt}} \sum_{t \in \mathcal{I}_{adapt}} \left\| \Phi_{AD}(\mathbf{q}_t^{(i)}, \mathbf{p}_t^{(i)}, \mathbf{u}_t^{(i)}; \theta_{AD}, \zeta_i) - [\mathbf{q}_{t+1}^{(i)}, \mathbf{p}_{t+1}^{(i)}] \right\|^2. \quad (6)$$

This ensures that  $\zeta_i$  adapts to system or task specific idiosyncrasies.

Once the local parameters  $\zeta_i$  have been adapted to the optimal value  $\zeta_i^*$ , we evaluate the model’s performance on  $\mathcal{I}_{meta}$  portion of the trajectory. The corresponding outer

loss:

$$\mathcal{L}_{outer}^{(i)} = \frac{1}{\mathcal{I}_{meta}} \sum_{t \in \mathcal{I}_{meta}} \left\| \Phi_{AD}(\mathbf{q}_t^{(i)}, \mathbf{p}_t^{(i)}, \mathbf{u}_t^{(i)}; \theta_{AD}, \zeta_i^*) - [\mathbf{q}_{t+1}^{(i)}, \mathbf{p}_{t+1}^{(i)}] \right\|^2, \quad (7)$$

propagates gradients *only* to  $\theta_{AD}$ . The overall training objective is then the sum over  $\mathcal{L}_{outer}^{(i)}$  for all systems  $i$ , over the batch.

We finalize the decoder with a Multi-Layer Perceptron (MLP) that outputs the position and momentum for the next time  $\{\hat{\mathbf{q}}_{t+1}^{(i)}, \hat{\mathbf{p}}_{t+1}^{(i)}\}$ . The architecture is then used autoregressively for future predictions.

### 3.3. Autoregressive Inference

Once both the SymplecticEncoder and ActiveDecoder (Sections 3.1 and 3.2) are trained, we generate future predictions by rolling out the model *autoregressively* during inference time. Specifically, at test time, we are given initial phase-space measurements. We first map to the conservative portion of the phase-space,  $(\mathbf{q}_t^{(i)}, \mathbf{p}_t^{(i)})$  through the SymplecticEncoder. The ActiveDecoder then produces the next predicted phase-space trajectory  $(\hat{\mathbf{q}}_{t+1}^{(i)}, \hat{\mathbf{p}}_{t+1}^{(i)})$ , based on the pipeline highlighted in Section 3.2. However, we subsequently treat  $(\hat{\mathbf{q}}_{t+1}^{(i)}, \hat{\mathbf{p}}_{t+1}^{(i)})$  as inputs for the next timesteps. This is repeated over the context window provided to the decoder.

In summary, by pairing our SymplecticEncoder (to ensure structure preservation) that provides a strong **inductive bias** with an *Autoregressive Transformer-style Decoder* (ActiveDecoder) equipped with *meta-attention* (to handle individual system variations) and end-to-end training with metalearning, our network, MetaSym, can rapidly adapt to diverse physical systems while guaranteeing physically consistent core dynamics. The following section presents a range of experimental results demonstrating superior performance compared to state-of-the-art approaches, especially in long-horizon stability and few-shot generalization to new system instances of varying complexity.

## 4. Results

In this section, we evaluate MetaSym’s performance, against a variety of State-of-The-Art (SoTA) models and benchmarks. In particular, we report the behavior of MetaSym against Transformers that have achieved impressive performance in modeling physical systems (Geneva & Zabaras, 2022) and DHNNs (Sosanya & Greydanus, 2022) that model systems via the Hemholtz decomposition, although they require gradient information and a numerical integrator to obtain trajectory data. Our model predicts the subsequent

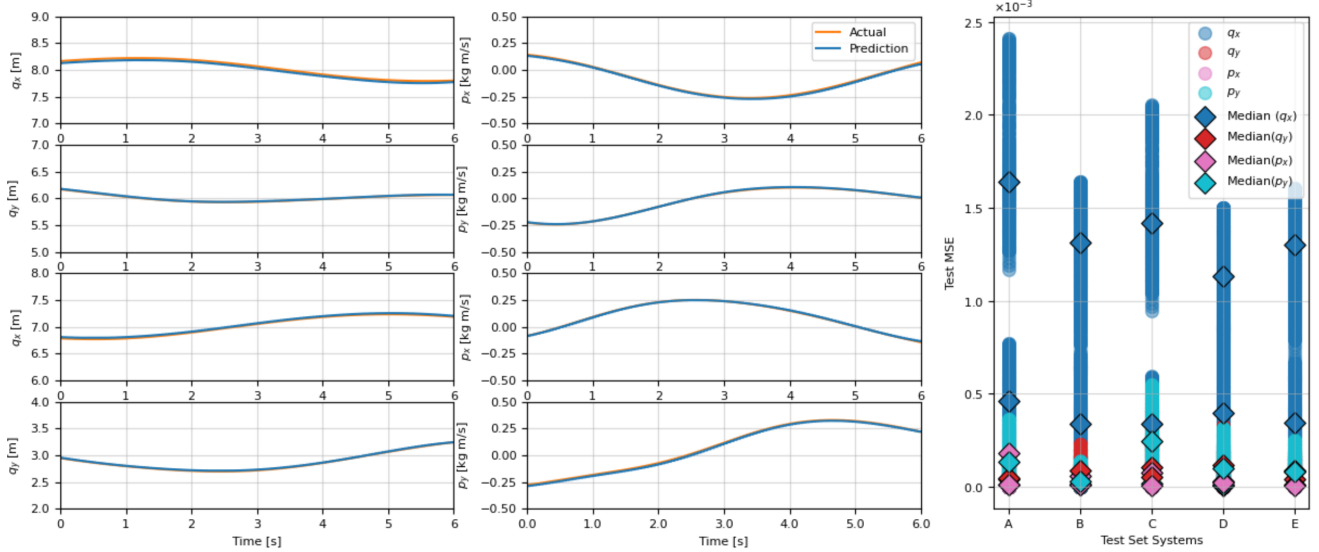


Figure 2. **(Left)** Represents the trajectory of the position and the momentum for arbitrary masses from the spring mesh system. The actual (orange line) and predicted (blue line) trajectories for the positions  $q_x$  and  $q_y$  along the  $x$  and  $y$  coordinates as well as the corresponding momenta ( $p_x, p_z$ ) are plotted. **(Right)** Plots the mean squared error of the trajectories for five random systems from the test set, along with each phase-space component’s median value.

timesteps directly, which poses a much harder task that does not require numerical integration, which can be time-consuming and may hinder real-time performance. These results also reflect on the effectiveness of our design choices.

As mentioned in Section 1.1, we choose to benchmark MetaSym for three extremely challenging and diverse datasets. Notably, we choose the spring mesh system, which tests scalability and closely resembles predicting the dynamics modeled using finite element methods. This dataset has provided the state-of-art testbed for large dimensional systems (Otness et al., 2021). We consider a novel dataset to demonstrate the robustness to noise and flexibility to model all types of physical systems with MetaSym by, considering an open quantum system undergoing heterodyne detection. Finally, we choose to predict the dynamics of a quadroto, a long standing benchmark in robotics and challenging due to floating base dynamics (Bansal et al., 2016). The description of each experimental setup is laid in the next sections, however a more extensive description can be found in Appendix B.

#### 4.1. Spring Mesh-System

For our first benchmark, we consider a 400 dimensional spring mesh system initially proposed by Otness et al. as part of the extensive benchmark for learning physical systems (Otness et al., 2021). The spring mesh system is provided as the most complex physical system among their benchmarks due to its high-dimensional state-space and dynamic couplings. This system is also used to model deformable volumes and the surfaces of complex objects that are vital to engineering tasks (Pfaff et al., 2021). In this

setup, each spring position is discretized by nodes whose position is updated based on forces computed from spring extensions and compressions, thus subjecting the simulation to nontrivial communication and computation patterns between different node positions. For a more in-depth description of the benchmark, refer to Appendix B.1.

#### 4.2. Open Quantum System

To benchmark MetaSym on a novel open quantum dynamics dataset, we consider a *parametric oscillator* initialized in a coherent state (Gardiner & Zoller, 2010). The system Hamiltonian includes three contributions: the harmonic term,  $\hat{H}_{osc} = \omega \hat{a}^\dagger \hat{a}$ , the squeezing term,  $\hat{H}_{sqz} = \frac{i\chi}{2} (\hat{a}^{\dagger 2} - \hat{a}^2)$ , and the cubic driving term,  $\hat{H}_{cubic} = \beta (\hat{a}^3 + \hat{a}^{\dagger 3})$ . Here,  $\hat{a}^\dagger$  and  $\hat{a}$  represent creation and annihilation operators in a truncated Fock space of dimension  $N$ . Dissipation arises due to coupling with a thermal bath at rate  $\gamma$  and average thermal occupation  $\langle n_{th} \rangle$ . We assume that the system is continuously monitored via heterodyne detection, leading to a stochastic master equation for the conditional quantum state (refer to Appendix B.2). The primary observables are the real and imaginary components (quadratures) of the heterodyne current, denoted  $X$  and  $P$ , respectively. For this benchmark, we generate the dataset by numerically solving the stochastic master equation for the setup described (Johansson et al., 2012). We produce a dataset with varying measurement efficiencies  $\eta$ , squeezing strength  $\chi$ , cubic term strength  $\beta$ , oscillator frequency  $\omega$  and average thermal occupation  $\langle n_{th} \rangle$  of the bath along with different initial states. This reflects real world experimental scenarios with variable  $\eta$  due to sensors or non ideal measurement condi-

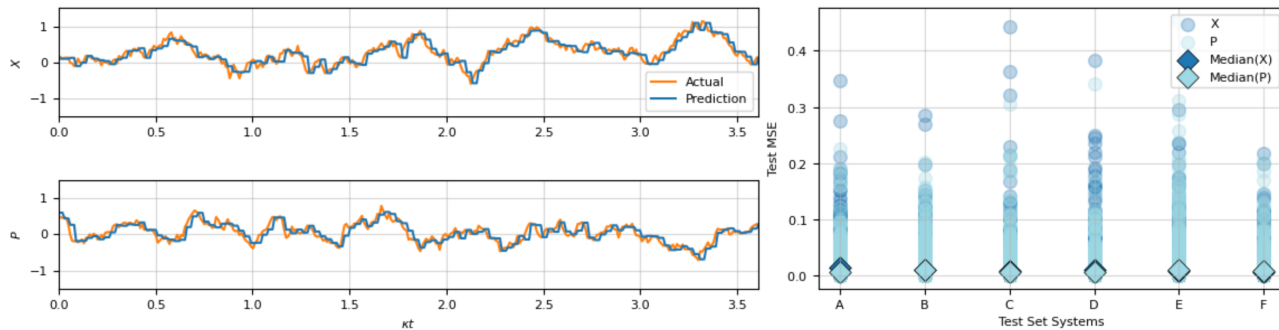


Figure 3. (Left) Represents the trajectory of the two measured quadratures obtained from heterodyne measurement for an arbitrary quantum system in the test set with measurement efficiency  $\eta = 0.86$  and measurement strength  $\kappa$ . The actual measurement trajectory (orange line) is plotted against the predicted measurement (blue line) by MetaSym. (Right) Plots the mean squared error of the trajectories along with the respective median value for five random systems with arbitrary initial states, and other randomized parameters from the test set.

tions. Refer to Appendix B.2 for a detailed description of the training setup and out-of-distribution inference setup that we used.

### 4.3. Quadrotor

For our final benchmark, we consider a quadrotor system, a well-known robotic platform with various applications across different domains, since the agility and speed of such systems are challenging for current SoTA data-driven methods (Sanyal & Roy, 2023). The complexity of the systems originate from the floating-base dynamics and the discontinuous orientation representation (Zhou et al., 2019). The floating-base dynamics are prone to internal covariate shift during the training of data-driven models, since the magnitudes of the phase-space can vary across systems and time. Simultaneously, representing the quadrotor’s orientation with Euler angles introduces singularities, while unit-quaternions have a nonlinear constraint on their total magnitude which most times is enforced using penalties in the loss function. This can often lead to local-minima that can dramatically slow down or stop the training progress. Our physics-informed SymplecticEncoder, along with the meta-learning capabilities of the ActiveDecoder, presents increased robustness across these problems. To avoid additional terms in the loss function, we project the quaternions representing the floating-base’s orientation to their respective tangent-space. For a more elaborate description of our simulation setup, refer to Appendix B.3.

### 4.4. Benchmarks

We evaluate our architecture’s accuracy and memory footprint against two state-of-the-art methods and a naive baseline: an auto-regressive Transformer model (Vaswani, 2017), a physics-informed DHNN model (Greydanus et al., 2019) and a Multilayered Perceptron (MLP). Both MetaSym and

the Transformer predict the next timestep autoregressively, while the DHNN estimates the symplectic and dissipative gradients and relies on an integrator to unroll the trajectory. Consequently, the DHNN is also unable to predict quadrature measurements since these derivatives are not well defined and involve a complex Wiener term (Milburn, 1987). Additionally, the DHNN’s training proved to be less stable as compared to MetaSym and the Transformer’s convergence properties. Finally, all models were tested in an autoregressive manner, in which each prediction is provided again as input to the model for the next timestep. As seen in Table 1, this study exposes the true performance capability and scalability of our architecture with the superior error accumulation over long horizon prediction of MetaSym. We achieve superior performance with smaller model sizes for MetaSym especially for high dimensional systems eg. spring mesh system. For the quantum dynamics benchmark, smaller models are crucial to achieve real-time prediction and control. Hardware limitations for quantum control restrict the use of larger models with higher latency. We demonstrate superior performance compared to the Transformer, the current state-of-the-art model (Vaidyanathan et al., 2024). Moreover, our model size falls below the threshold for real-time predictions of quantum devices (Reuer et al., 2023).

## 5. Conclusion & Future Work

In this work, we introduced **MetaSym**, a novel deep-learning framework that combines structure-preserving symplectic networks with an autoregressive, decoder equipped with meta-learning for modeling a wide range of physical systems. The core idea rests on striking a balance between *strong physical priors*—namely the intrinsic symplectic structure of Hamiltonian mechanics—and the *flexibility* required to capture non-conservative effects and heterogeneous system parameters. Our experimental results across

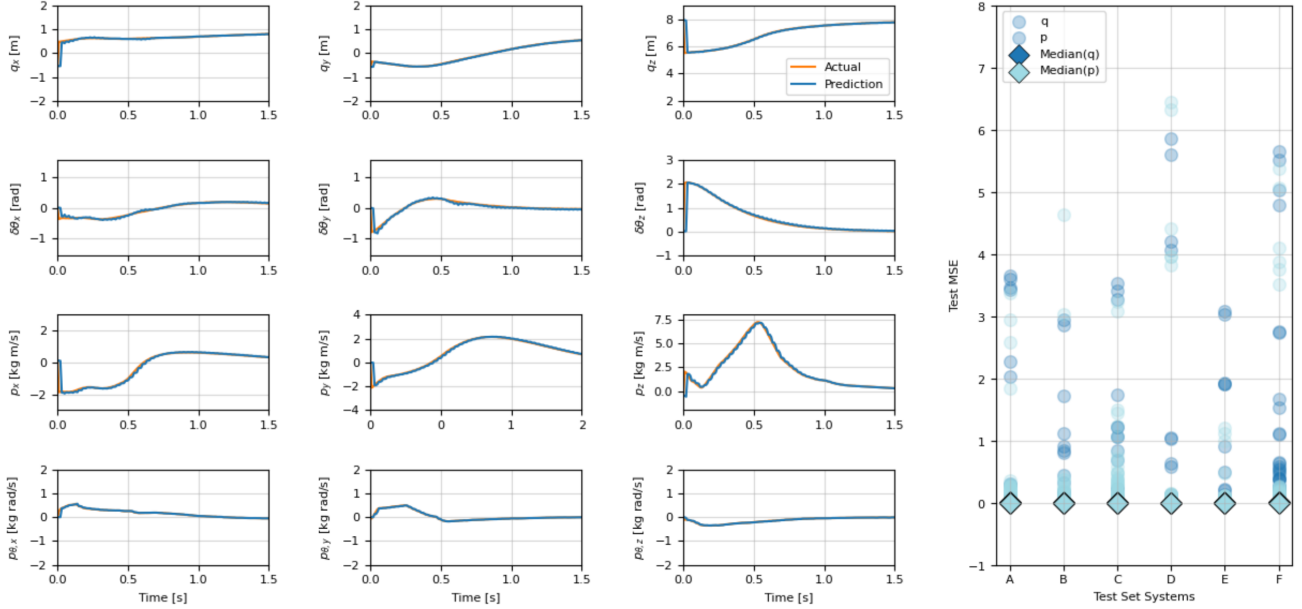


Figure 4. (Left) Represents the translational and angular phase-space evolution of the quadrotor, with training and test trajectories generated using the *Crocodyl* trajectory optimization package (Mastalli et al., 2020). Each task is initialized with randomized initial conditions and a randomized terminal position over a 1.5s horizon. The ground-truth test trajectory (orange line) is compared to MetaSym’s predictions (blue line) indicating the good predictive capabilities of our model. (Right) Plots the average mean squared error of the trajectories for five randomly generated test-set systems with arbitrary initial conditions and terminal positions, along with randomized inertial system parameters.

Table 1. Trajectory error and parameter count against SoTA baselines for three out-of-distribution datasets

Models	Spring Mesh System		Quantum System		Quadrotor	
	Param. Count	Trajectory MSE ( $\pm\sigma$ )	Param. Count	Trajectory MSE ( $\pm\sigma$ )	Param. Count	Trajectory MSE ( $\pm\sigma$ )
DHNNs	3.0M	32.468 (28.086)	N/A	N/A	3138	26.375 (9.160)
Transformer	3.2M	36.653 (15.618)	194	0.950 (0.239)	4680	34.584 (14.063)
Naive Baseline (MLP)	3.5M	323.199 (13.959)	262	0.898 (0.226)	4012	39.311 (13.937)
MetaSym (ours)	<b>2.9M</b>	<b>19.233 (15.673)</b>	<b>130</b>	<b>0.859 (0.215)</b>	<b>3036</b>	<b>25.889 (8.967)</b>

diverse domains—ranging from high-dimensional spring-mesh dynamics to open quantum systems and robotics-inspired quadrotor models—demonstrated that MetaSym outperforms state-of-the-art baselines in both long-horizon accuracy and few-shot adaptation with smaller model sizes.

From a geometric perspective, the SymplecticEncoder approximates canonical flows while preserving key invariants, significantly mitigating energy drift and ensuring robust long-term predictions. The encoder’s invertible design enforces time-reversal symmetry and reduces error accumulation. Meanwhile, the ActiveDecoder models departures from ideal Hamiltonian evolution through autoregressive prediction and meta-attention. The resulting architecture is computationally efficient, given that it does not require explicit numerical integration during inference, and—through meta-learning—readily adapts to system variations with minimal additional data. This approach offers a scalable

and unified framework for high-fidelity physics modeling in realistic settings with provable near symplectic properties (see Appendix C.4).

Considering MetaSym’s promising performance, we seek to investigate several future directions such as incorporating a fully symplectic network for modeling realistic physics by exploiting the underlying structure of noise and our control signals. Another natural extension of few-shot adaptation is online learning and control. Since MetaSym can quickly adapt to new system configurations with minimal data, this capability can be leveraged in real-time control loops and model-based Reinforcement Learning (RL) algorithms. Future research can investigate how to integrate the decoder’s adaptation step with RL or adaptive Model Predictive Control (MPC) frameworks, effectively enabling self-tuning controllers in rapidly changing environments.

## Acknowledgments

The authors would like to thank Lucas Schorling, Federico Fedele and Vivek Wadhia for the useful discussions. P.V. is supported by the United States Army Research Office under Award No. W911NF-21-S-0009-2. A.P is supported by University of Oxford’s Clarendon Fund. M.T.M. is supported by a Royal Society University Research Fellowship. N.A. acknowledges support from the European Research Council (grant agreement 948932) and the Royal Society (URF-R1-191150).

## References

- Alexeev, Y., Farag, M. H., Patti, T. L., Wolf, M. E., Ares, N., Aspuru-Guzik, A., Benjamin, S. C., Cai, Z., Chandani, Z., Fedele, F., Harrigan, N., Kim, J.-S., Kyoseva, E., Lietz, J. G., Lubowe, T., McCaskey, A., Melko, R. G., Nakaji, K., Peruzzo, A., Stanwyck, S., Tubman, N. M., Wang, H., and Costa, T. Artificial intelligence for quantum computing, 2024. URL <https://arxiv.org/abs/2411.09131>.
- Ares, N. Machine learning as an enabler of qubit scalability. *Nature Reviews Materials*, 6(10):870–871, 2021.
- Bai, K., Zhang, L., Chen, Z., Wan, F., and Zhang, J. Close the sim2real gap via physically-based structured light synthetic data simulation, 2024. URL <https://arxiv.org/abs/2407.12449>.
- Bansal, S., Akametalu, A. K., Jiang, F. J., Laine, F., and Tomlin, C. J. Learning quadrotor dynamics using neural network for flight control. In *2016 IEEE 55th Conference on Decision and Control (CDC)*, pp. 4653–4660. IEEE, 2016.
- Bausch, J., Senior, A. W., Heras, F. J., Edlich, T., Davies, A., Newman, M., Jones, C., Satzinger, K., Niu, M. Y., Blackwell, S., et al. Learning high-accuracy error decoding for quantum processors. *Nature*, pp. 1–7, 2024.
- Carleo, G., Cirac, I., Cranmer, K., Daudet, L., Schuld, M., Tishby, N., Vogt-Maranto, L., and Zdeborová, L. Machine learning and the physical sciences. *Rev. Mod. Phys.*, 91:045002, Dec 2019. doi: 10.1103/RevModPhys.91.045002. URL <https://link.aps.org/doi/10.1103/RevModPhys.91.045002>.
- Chen, R. T. Q., Rubanova, Y., Bettencourt, J., and Duvenaud, D. Neural ordinary differential equations, 2019. URL <https://arxiv.org/abs/1806.07366>.
- Chen, Z., Zhang, J., Arjovsky, M., and Bottou, L. Symplectic recurrent neural networks, 2020. URL <https://arxiv.org/abs/1909.13334>.
- Choe, S. K., Mehta, S. V., Ahn, H., Neiswanger, W., Xie, P., Strubell, E., and Xing, E. Making scalable meta learning practical, 2023. URL <https://arxiv.org/abs/2310.05674>.
- Cranmer, M., Greydanus, S., Hoyer, S., Battaglia, P., Spergel, D., and Ho, S. Lagrangian neural networks, 2020. URL <https://arxiv.org/abs/2003.04630>.
- Finn, C., Abbeel, P., and Levine, S. Model-agnostic meta-learning for fast adaptation of deep networks, 2017. URL <https://arxiv.org/abs/1703.03400>.
- Flurin, E., Martin, L. S., Hacothen-Gourgy, S., and Siddiqi, I. Using a recurrent neural network to reconstruct quantum dynamics of a superconducting qubit from physical observations. *Phys. Rev. X*, 10:011006, Jan 2020. doi: 10.1103/PhysRevX.10.011006. URL <https://link.aps.org/doi/10.1103/PhysRevX.10.011006>.
- Gardiner, C. W. and Zoller, P. *Quantum Noise: A Handbook of Markovian and Non-Markovian Quantum Stochastic Methods with Applications to Quantum Optics*. Springer Series in Synergetics. Springer, Berlin Heidelberg, 3. ed., [nachdr.] edition, 2010. ISBN 978-3-540-22301-6.
- Gebhart, V., Santagati, R., Gentile, A. A., Gauger, E. M., Craig, D., Ares, N., Banchi, L., Marquardt, F., Pezzè, L., and Bonato, C. Learning quantum systems. *Nature Reviews Physics*, 5(3):141–156, 2023.
- Geisert, M. and Mansard, N. Trajectory generation for quadrotor based systems using numerical optimal control. In *2016 IEEE International Conference on Robotics and Automation (ICRA)*, pp. 2958–2964, 2016. doi: 10.1109/ICRA.2016.7487460.
- Geneva, N. and Zabararas, N. Transformers for modeling physical systems. *Neural Networks*, 146:272–289, February 2022. ISSN 0893-6080. doi: 10.1016/j.neunet.2021.11.022. URL <http://dx.doi.org/10.1016/j.neunet.2021.11.022>.
- Ghadami, A. and Epureanu, B. I. Data-driven prediction in dynamical systems: recent developments. *Philosophical Transactions of the Royal Society A*, 380(2229):20210213, 2022.
- Greydanus, S., Dzamba, M., and Yosinski, J. Hamiltonian neural networks, 2019. URL <https://arxiv.org/abs/1906.01563>.
- Jacobs, K. and Steck, D. A. A straightforward introduction to continuous quantum measurement. *Contemporary Physics*, 47(5):279–303, September 2006. ISSN 1366-5812. doi: 10.1080/00107510601101934. URL <http://dx.doi.org/10.1080/00107510601101934>.

- Jin, P., Zhang, Z., Zhu, A., Tang, Y., and Karniadakis, G. E. Sympnets: Intrinsic structure-preserving symplectic networks for identifying hamiltonian systems, 2020. URL <https://arxiv.org/abs/2001.03750>.
- Johansson, J., Nation, P., and Nori, F. Qutip: An open-source python framework for the dynamics of open quantum systems. *Computer Physics Communications*, 183(8):1760–1772, August 2012. ISSN 0010-4655. doi: 10.1016/j.cpc.2012.02.021. URL <http://dx.doi.org/10.1016/j.cpc.2012.02.021>.
- Kibble, T. and Berkshire, F. H. *Classical mechanics*. world scientific publishing company, 2004.
- Li, Q., Wang, T., Roychowdhury, V., and Jawed, M. K. Metalearning generalizable dynamics from trajectories. *Phys. Rev. Lett.*, 131:067301, Aug 2023. doi: 10.1103/PhysRevLett.131.067301. URL <https://link.aps.org/doi/10.1103/PhysRevLett.131.067301>.
- Li, W., Zou, L., Tang, M., Yu, Q., Li, W., and Li, C. Meta-lora: Memory-efficient sample reweighting for fine-tuning large language models. In *Proceedings of the 31st International Conference on Computational Linguistics*, pp. 8504–8517, 2025.
- Li, Z., Kovachki, N., Azizzadenesheli, K., Liu, B., Bhattacharya, K., Stuart, A., and Anandkumar, A. Fourier neural operator for parametric partial differential equations, 2021. URL <https://arxiv.org/abs/2010.08895>.
- Manzano, D. A short introduction to the lindblad master equation. *AIP Advances*, 10(2), February 2020. ISSN 2158-3226. doi: 10.1063/1.5115323. URL <http://dx.doi.org/10.1063/1.5115323>.
- Mastalli, C., Budhiraja, R., Merkt, W., Saurel, G., Ham-moud, B., Naveau, M., Carpentier, J., Righetti, L., Vijayakumar, S., and Mansard, N. Crocodyl: An Efficient and Versatile Framework for Multi-Contact Optimal Control. In *IEEE International Conference on Robotics and Automation (ICRA)*, 2020.
- Milburn, G. J. Quantum measurement theory of optical heterodyne detection. *Phys. Rev. A*, 36: 5271–5279, Dec 1987. doi: 10.1103/PhysRevA.36.5271. URL <https://link.aps.org/doi/10.1103/PhysRevA.36.5271>.
- Nichol, A. On first-order meta-learning algorithms. *arXiv preprint arXiv:1803.02999*, 2018.
- Okamoto, Y. and Kojima, R. Learning deep dissipative dynamics, 2024. URL <https://arxiv.org/abs/2408.11479>.
- Otness, K., Gjoka, A., Bruna, J., Panozzo, D., Peherstorfer, B., Schneider, T., and Zorin, D. An extensible benchmark suite for learning to simulate physical systems, 2021. URL <https://arxiv.org/abs/2108.07799>.
- Papatheodorou, A., Merkt, W., Mitchell, A. L., and Havoutis, I. Momentum-aware trajectory optimisation using full-centroidal dynamics and implicit inverse kinematics. In *2024 IEEE/RSJ International Conference on Intelligent Robots and Systems (IROS)*, pp. 11940–11947, 2024. doi: 10.1109/IROS58592.2024.10801374.
- Pfaff, T., Fortunato, M., Sanchez-Gonzalez, A., and Battaglia, P. W. Learning mesh-based simulation with graph networks, 2021. URL <https://arxiv.org/abs/2010.03409>.
- Rajeswaran, A., Finn, C., Kakade, S. M., and Levine, S. Meta-learning with implicit gradients. *Advances in neural information processing systems*, 32, 2019.
- Reuer, K., Landgraf, J., Fösel, T., O’Sullivan, J., Beltrán, L., Akin, A., Norris, G. J., Remm, A., Kerschbaum, M., Besse, J.-C., Marquardt, F., Wallraff, A., and Eichler, C. Realizing a deep reinforcement learning agent for real-time quantum feedback. *Nature Communications*, 14(1), November 2023. ISSN 2041-1723. doi: 10.1038/s41467-023-42901-3. URL <http://dx.doi.org/10.1038/s41467-023-42901-3>.
- Royer, A. Wigner function in liouville space: a canonical formalism. *Physical Review A*, 43(1):44, 1991.
- Sanyal, S. and Roy, K. Ramp-net: A robust adaptive mpc for quadrotors via physics-informed neural network, 2023. URL <https://arxiv.org/abs/2209.09025>.
- Sosanya, A. and Greydanus, S. Dissipative hamiltonian neural networks: Learning dissipative and conservative dynamics separately, 2022. URL <https://arxiv.org/abs/2201.10085>.
- Vaidhyanathan, P., Marquardt, F., Mitchison, M. T., and Ares, N. Quantum feedback control with a transformer neural network architecture, 2024. URL <https://arxiv.org/abs/2411.19253>.
- Vaswani, A. Attention is all you need. *Advances in Neural Information Processing Systems*, 2017.
- Zhang, X., Wang, L., Helwig, J., Luo, Y., Fu, C., Xie, Y., Liu, M., Lin, Y., Xu, Z., Yan, K., Adams, K., Weiler, M., Li, X., Fu, T., Wang, Y., Yu, H., Xie, Y., Fu, X., Strasser, A., Xu, S., Liu, Y., Du, Y., Saxton, A., Ling, H., Lawrence, H., Stärk, H., Gui, S., Edwards, C., Gao, N., Ladera, A., Wu, T., Hofgard, E. F., Tehrani, A. M., Wang, R., Daigavane, A., Bohde, M., Kurtin, J., Huang, Q., Phung, T., Xu, M., Joshi, C. K., Mathis, S. V., Azizzadenesheli,

K., Fang, A., Aspuru-Guzik, A., Bekkers, E., Bronstein, M., Zitnik, M., Anandkumar, A., Ermon, S., Liò, P., Yu, R., Günnemann, S., Leskovec, J., Ji, H., Sun, J., Barzilay, R., Jaakkola, T., Coley, C. W., Qian, X., Qian, X., Smidt, T., and Ji, S. Artificial intelligence for science in quantum, atomistic, and continuum systems, 2024. URL <https://arxiv.org/abs/2307.08423>.

Zhong, Y. D., Dey, B., and Chakraborty, A. Dissipative symplectic: Encoding hamiltonian dynamics with dissipation and control into deep learning, 2020. URL <https://arxiv.org/abs/2002.08860>.

Zhong, Y. D., Dey, B., and Chakraborty, A. Symplectic ode-net: Learning hamiltonian dynamics with control, 2024. URL <https://arxiv.org/abs/1909.12077>.

Zhou, Y., Barnes, C., Lu, J., Yang, J., and Li, H. On the continuity of rotation representations in neural networks. In *2019 IEEE/CVF Conference on Computer Vision and Pattern Recognition (CVPR)*, pp. 5738–5746, 2019. doi: 10.1109/CVPR.2019.00589.

Zintgraf, L., Shiarli, K., Kurin, V., Hofmann, K., and Whiteson, S. Fast context adaptation via meta-learning. In *International Conference on Machine Learning*, pp. 7693–7702. PMLR, 2019a.

Zintgraf, L. M., Shiarlis, K., Kurin, V., Hofmann, K., and Whiteson, S. Fast context adaptation via meta-learning, 2019b. URL <https://arxiv.org/abs/1810.03642>.

## A. Meta Learning Setup

As mentioned in Section 3, we elaborate on the algorithmic pipeline of our SymplecticEncoder and ActiveDecoder modules. In particular, we outline the MAML-based meta-learning strategy for the SymplecticEncoder and the inner-outer adaptation meta-learning for the ActiveDecoder. Figure 5 provides an interpretable insight into the effect of inner adaptation during the meta-update step and its effectiveness.

### A.1. Encoder

Following Section 3.1, Algorithm 1 provides a high-level overview of how the SymplecticEncoder is trained via meta-learning.

---

#### Algorithm 1 Meta-Learning for the SymplecticEncoder

---

**Require:**  $\mathcal{D} = \{\mathcal{D}^{(1)}, \dots, \mathcal{D}^{(N)}\}$ : Training data from  $N$  related systems. Each  $\mathcal{D}^{(i)}$  is a trajectory of states  $(\mathbf{q}_t^{(i)}, \mathbf{p}_t^{(i)}, \mathbf{u}_t^{(i)})_{t=1}^T$ .

- 1: **for** epoch = 1  $\rightarrow$   $N_{\text{epochs}}$  **do**
- 2:   **for** each mini-batch of systems  $B \subseteq \{1, \dots, N\}$  **do**
- 3:     optimizer\_theta.zero\_grad()
- 4:     inner\_optimizer.zero\_grad()
- 5:     **for** each system  $i \in B$  **do**
- 6:       **Split the trajectory  $\mathcal{D}^{(i)}$  into:**
- 7:        $\mathcal{I}_{\text{adapt}} \subset \{1, \dots, T_i\}$ ,  $\mathcal{I}_{\text{meta}} = \{1, \dots, T_i\} \setminus \mathcal{I}_{\text{adapt}}$ .
- 8:        $\mathcal{L}_{\text{meta}} \leftarrow 0$
- 9:       **Fast Adaptation: Adapt system-specific parameters**
- 10:        $\theta_{SE}^{(i)} \leftarrow \theta_{SE}.\text{clone}().\text{detach}()$  {Detach}
- 11:       **for**  $k = 1 \rightarrow K$  **do**
- 12:         inner\_optimizer.zero\_grad()
- 13:          $\mathcal{L}_{\text{inner}}^{(i)} \leftarrow 0$
- 14:         **for**  $t \in \mathcal{I}_{\text{adapt}}$  **do**
- 15:            $(\hat{\mathbf{q}}_{t+1}^{(i)}, \hat{\mathbf{p}}_{t+1}^{(i)}) \leftarrow \Phi_{SE}(\mathbf{q}_t^{(i)}, \mathbf{p}_t^{(i)}, \mathbf{u}_t^{(i)}; \theta_{SE}^{(i)})$
- 16:            $\mathcal{L}_{\text{inner}}^{(i)} += \|\hat{\mathbf{q}}_{t+1}^{(i)}, \hat{\mathbf{p}}_{t+1}^{(i)} - [\mathbf{q}_{t+1}^{(i)}, \mathbf{p}_{t+1}^{(i)}]\|^2$
- 17:         **end for**
- 18:          $\mathcal{L}_{\text{inner}}^{(i)}.\text{backward}()$
- 19:         inner\_optimizer.step() {Update  $\theta_{SE}^{(i)}$  only}
- 20:       **end for**
- 21:       **Meta Update: Update the global parameters  $\theta_{AD}$**
- 22:       **for**  $t \in \mathcal{I}_{\text{meta}}$  **do**
- 23:          $\theta_{SE} \leftarrow \theta_{SE}^{(i)*}.\text{clone}()$  {No Detach}
- 24:          $(\hat{\mathbf{q}}_{t+1}^{(i)}, \hat{\mathbf{p}}_{t+1}^{(i)}) \leftarrow \Phi_{SE}(\mathbf{q}_t^{(i)}, \mathbf{p}_t^{(i)}, \mathbf{u}_t^{(i)}; \theta_{SE})$
- 25:          $\mathcal{L}_{\text{meta}} += \|\hat{\mathbf{q}}_{t+1}^{(i)}, \hat{\mathbf{p}}_{t+1}^{(i)} - [\mathbf{q}_{t+1}^{(i)}, \mathbf{p}_{t+1}^{(i)}]\|^2$
- 26:       **end for**
- 27:     **end for**
- 28:      $\mathcal{L}_{\text{meta}}.\text{backward}()$  {Eq. (5)}
- 29:     optimizer\_theta.step() {Update  $\theta_{SE}$  only}
- 30:   **end for**
- 31: **end for**

---

## A.2. Decoder

Algorithm 2 provides a high-level overview of how the ActiveDecoder is trained via meta-learning.

---

### Algorithm 2 Meta-Learning for the ActiveDecoder

---

**Require:**  $\mathcal{D} = \{\mathcal{D}^{(1)}, \dots, \mathcal{D}^{(N)}\}$ : Training data from  $N$  related systems. Each  $\mathcal{D}^{(i)}$  is a trajectory of states

```

 $(\mathbf{q}_t^{(i)}, \mathbf{p}_t^{(i)}, \mathbf{u}_t^{(i)})_{t=1}^T$ .
1: for epoch = 1  $\rightarrow N_{\text{epochs}}$  do
2:   for each mini-batch of systems  $B \subseteq \{1, \dots, N\}$  do
3:     optimizer_theta.zero_grad()
4:     for each system  $i \in B$  do
5:       Split the trajectory  $\mathcal{D}^{(i)}$  into:
6:          $\mathcal{I}_{\text{adapt}} \subset \{1, \dots, \mathcal{T}_i\}$ ,  $\mathcal{I}_{\text{meta}} = \{1, \dots, \mathcal{T}_i\} \setminus \mathcal{I}_{\text{adapt}}$ .
7:       Inner loop: Adapt local parameters  $\zeta_i$ 
8:       for  $k = 1 \rightarrow K$  do
9:         for  $t \in \mathcal{I}_{\text{adapt}}$  do
10:          inner_optimizer.zero_grad()
11:           $\zeta_i$ .randomize() {Reinitialize  $\zeta_i$ }
12:           $(\hat{\mathbf{q}}_{t+1}^{(i)}, \hat{\mathbf{p}}_{t+1}^{(i)}) \leftarrow \Phi_{\text{AD}}(\mathbf{q}_t^{(i)}, \mathbf{p}_t^{(i)}, \mathbf{u}_t^{(i)}; \theta_{\text{AD}}, \zeta_i)$ 
13:           $\mathcal{L}_{\text{inner}}^{(i)} = \|\hat{\mathbf{q}}_{t+1}^{(i)} - \mathbf{q}_{t+1}^{(i)}\|^2$ 
14:           $\mathcal{L}_{\text{inner}}^{(i)}$ .backward() {Eq. (3.2)}
15:          inner_optimizer.step() {Update  $\zeta_i$  only}
16:        end for
17:      end for
18:      Outer loop: Meta-update for the global parameters  $\theta_{\text{AD}}$ 
19:      optimizer_theta.zero_grad() {No update to  $\zeta_i$  now}
20:       $\mathcal{L}_{\text{outer}}^{(i)} \leftarrow 0$ 
21:      for  $t \in \mathcal{I}_{\text{meta}}$  do
22:         $(\hat{\mathbf{q}}_{t+1}^{(i)}, \hat{\mathbf{p}}_{t+1}^{(i)}) \leftarrow \Phi_{\text{AD}}(\mathbf{q}_t^{(i)}, \mathbf{p}_t^{(i)}, \mathbf{u}_t^{(i)}; \theta_{\text{AD}}, \zeta_i^*)$ 
23:         $\mathcal{L}_{\text{outer}}^{(i)} += \|\hat{\mathbf{q}}_{t+1}^{(i)} - \mathbf{q}_{t+1}^{(i)}\|^2$ 
24:      end for
25:       $\mathcal{L}_{\text{outer}}^{(i)}$ .backward() {Eq. (3.2)}
26:      optimizer_theta.step() {Update  $\theta_{\text{AD}}$  only}
27:    end for
28:  end for
29: end for

```

---

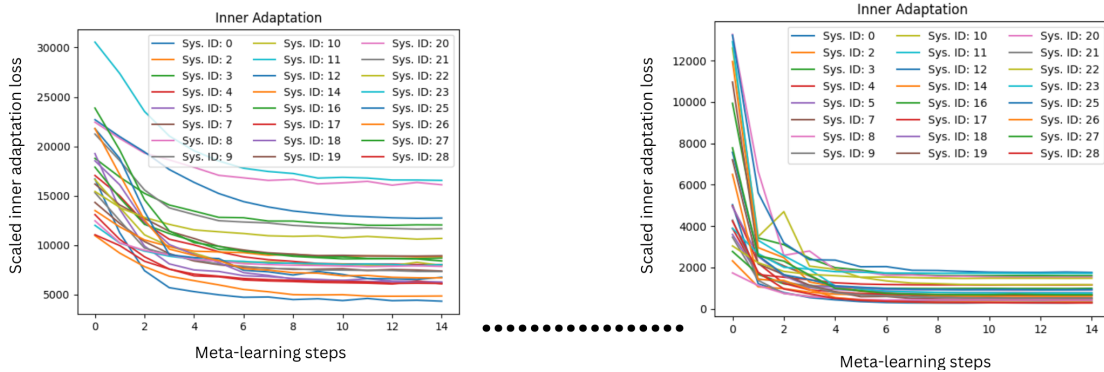


Figure 5. Represents the change in loss between training steps due to the meta-update of parameters.

## B. Experimental Setup

### B.1. Spring Mesh System

Spring networks are a simple proxy for numerous physical scenarios involving deformable solids and cloth (in computer graphics, mechanics, or robotics). Each pair of connected particles exchanges spring forces that depend on displacements from rest lengths. Viscous damping terms further shape the evolution. While the individual force law (Hooke’s law) is straightforward, the combination of hundreds of coupled springs can give rise to complex large-scale deformations and oscillations. By benchmarking on a spring mesh, we can examine how MetaSym learns large deformations, wave propagation through a membrane, or the impact of damping.

The training dataset consists of 25 distinct spring-mesh systems, each characterized by a unique set of physical parameters, including spring stiffness, damping coefficients, and initial conditions as indicated by Table 2. These parameters are sampled from a predefined distribution to ensure sufficient diversity within the training set. Each system is simulated over a time span of 2000 irregular timesteps, capturing the full trajectory of node displacements and momenta. The resulting dataset provides a rich representation of dynamical behaviors within the parameter space.

To assess generalization and robustness, we construct a validation dataset comprising 10 additional spring-mesh systems. Unlike the training set, the parameters for these systems are drawn from distributions that differ from those used during training as indicated by Table 3, introducing a domain shift that mimics real-world variations. This OOD validation set enables a rigorous evaluation of the model’s ability to extrapolate beyond the observed training dynamics and adapt to unseen conditions. For further information regarding the spring-mesh benchmark refer to (Otness et al., 2021).

By incorporating both in-distribution training data and OOD validation data, this experimental setup ensures a comprehensive assessment of the model’s learning capacity, robustness, and generalization performance when applied to novel physical configurations.

Parameters	Values
$\gamma_{decay}$ [kg/s]	Uniform(0.1, 0.2)
mass [kg]	Uniform(0.1, 2.0)
$K_{spring}$ [N/m]	Uniform(0.001, 0.5)
initial perturbations [m]	Uniform(0, 0.6)
dt [s]	Uniform(0.001, 0.03)

Table 2. In-distribution parameters  $T = 2000$ .

Parameters	Values
$\gamma_{decay}$ [kg/s]	Uniform(0.01, 0.05)
mass [kg]	Uniform(3.0, 5.0)
$K_{spring}$ [N/m]	Uniform(1.0, 3.0)
initial perturbations [m]	Uniform(0.9, 2.5)
dt [s]	Uniform(0.1, 0.3)

Table 3. Out-of-distribution parameters,  $T = 2000$

### B.2. Open Quantum System Derivation

Understanding the behavior of quantum systems plays a vital role in the development of promising technologies such as quantum computing, metrology, and sensing. While deep learning has found great success in several areas such as quantum control (Vaidhyanathan et al., 2024), error correction (Bausch et al., 2024) and tuning (Ares, 2021; Gebhart et al., 2023), predicting the measurement record based on modeling quantum dynamics has long remained elusive. In many scenarios, the system of interest is *open*: it couples to an environment (or bath) that can introduce thermal noise and dissipation. Furthermore, continuous monitoring (e.g., via homodyne detection) adds additional *measurement backaction*, reflecting fundamental constraints from quantum mechanics (Jacobs & Steck, 2006). Capturing these noise and measurement effects is pivotal for accurately predicting quantum trajectories and devising robust control protocols.

Unlike closed Hamiltonian evolutions, open quantum systems require one to solve Stochastic Master Equations (SMEs) incorporating decoherence and measurement terms. These equations produce trajectories of the (mixed) quantum state conditioned on the noisy measurement record. In many practical settings, however, we only have direct access to certain observables (e.g., position and momentum quadratures) rather than the full quantum state. Hence, training a deep learning network to model the quantum system and to predict future measurement outcomes becomes a natural and practically relevant challenge. The SME describes the evolution of the *conditioned* quantum state  $\rho_c(t)$  under the effect of environmental and measurement noise as (Jacobs & Steck, 2006)

$$d\rho_c(t) = -i[H, \rho_c(t)]dt + \sum_j \mathcal{D}[\hat{L}_j]\rho_c(t)dt + \sqrt{\eta}\mathcal{H}[\hat{M}]\rho_c(t)dW_t, \quad (8)$$

where the *dissipator* is  $\mathcal{D}[\hat{L}]\rho = \hat{L}\rho\hat{L}^\dagger - \frac{1}{2}\{\hat{L}^\dagger\hat{L}, \rho\}$ . Each Linblad operator,  $\hat{L}_j$ , represents a *collapse operator* that encodes coupling to the environment (e.g., photon loss to a reservoir, thermal excitations, dephasing, etc.) (Manzano, 2020). The stochastic backaction term,  $\mathcal{H}[\hat{M}]\rho = \hat{M}\rho + \rho\hat{M}^\dagger - \text{Tr}\left[\left(\hat{M} + \hat{M}^\dagger\right)\rho\right]\rho$ , describes continuous monitoring of an observable  $\hat{M}$ , with  $\eta$  the measurement efficiency ( $0 \leq \eta \leq 1$ ). The Wiener increment,  $dW_t$ , captures the randomness inherent in quantum measurement outcomes.

### B.2.1. SETUP FOR PARAMETRIC OSCILLATOR

In Section 4.2, we focus on a single-mode bosonic system with annihilation operator  $\hat{a}$  and creation operator  $\hat{a}^\dagger$ . The Hamiltonian is:

$$H = \omega\hat{a}^\dagger\hat{a} + \frac{i\chi}{2}(\hat{a}^{\dagger 2} - \hat{a}^2) + \beta(\hat{a}^3 + \hat{a}^{\dagger 3}), \quad (9)$$

with  $\omega$ ,  $\chi$  and  $\beta$  being the oscillator frequency, squeezing strength and cubic driving term respectively. We also include two Linblad operators:

$$\hat{L}_1 = \sqrt{\gamma(\bar{n}_{th} + 1)}\hat{a}, \quad \hat{L}_2 = \sqrt{\gamma\bar{n}_{th}}\hat{a}^\dagger, \quad (10)$$

where  $\gamma$  is the coupling rate to the thermal bath, and  $\bar{n}_{th}$  is the average occupation number.

A common measurement technique often employed in experimental settings is called heterodyne measurement. Heterodyne detection continuously measures both quadratures of the output of our dissipative qubit by mixing it with a local oscillator at a slightly shifted frequency and then demodulating the resulting beat signal. This yields two simultaneous photocurrents, often referred to as the in-phase ( $I$ ) and quadrature ( $Q$ ) components. This reflects a key practical outcome of solving Eq. (8) is that  $\rho_c(t)$  depends on this random measurement trajectory.

We employ heterodyne detection of the field operator  $\hat{a}$ . Based on this measurement scheme, we can get separate the real and imaginary parts to obtain quadrature values that roughly correspond to  $X$  and  $P$  while adding quantum noise and measurement uncertainties due to quantum mechanical effect (Flurin et al., 2020).

In the following Tables 5 and 4, we describe the parameters used to generate our dataset by solving the SME in order to generate training data.

Parameters	Values
oscillator frequency $\omega$	Uniform(0.5, 1.0)
squeezing strength $\chi$	Uniform(0.1, 0.4)
thermal occupation $\langle n_{th} \rangle$	Uniform(0.1, 0.5)
meas. efficiency $\eta$	Uniform(0.7, 1.0)

Table 4. In-distribution parameters  $dt = 0.5, T = 600$ .

Parameters	Values
oscillator frequency $\omega$	Uniform(0.1, 0.4)
squeezing strength $\chi$	Uniform(0.5, 0.8)
thermal occupation $\langle n_{th} \rangle$	Uniform(0.6, 0.7)
meas. efficiency $\eta$	Uniform(0.4, 0.6)

Table 5. Out-of-distribution parameters  $dt = 0.5, T = 600$

### B.3. Quadrotor

The quadrotor system challenges data-driven methods with its floating-base dynamics. To generate the training and OOD validation datasets we use *Crocodyl* trajectory optimization package based on the dynamics model proposed by (Geisert & Mansard, 2016). The training dataset comprises 30 systems with randomized parameters such as inertia, torque constant and rotor lengths as indicated in Table 6. Each trajectory is generated from a randomized initial condition to a random terminal position with zero velocity, within a pre-set bounding box, to avoid unrealistic velocities.

In the same manner the OOD validation set contains 10 trajectories, each one corresponding to a system with parameters drawn from the distributions indicated in Table 7.

Parameters	Values
Inertia $\mathcal{I}_{diag}$	Uniform(0.1, 0.2)
mass (m)	Uniform(0.5, 3.0)
$d_{cogs}$	Uniform(0.2, 0.5)
$C_{torques}$	Uniform(0.001, 0.1)

 Table 6. In-distribution parameters  $dt = 0.01, T = 250$ .

Parameters	Values
Inertia $\mathcal{I}_{diag}$	Uniform(0.3, 0.7)
mass (m)	Uniform(3.0, 5.0)
$d_{cogs}$	Uniform(0.5, 0.7)
$C_{torques}$	Uniform(0.1, 0.2)

 Table 7. Out-of-distribution parameters  $dt = 0.01, T = 500$ 

## C. Near Symplectic Architecture

In this section, we prove that composing our SymplecticEncoder  $\Phi_{\theta_{SE}}$  with our ActiveDecoder  $\Phi_{\theta_{AD}}$  handling control signals and dissipative effects yields a near-symplectic map, with an explicit bound on preserving approximate symplectic geometry. This formalizes the realistic effects we can introduce to MetaSym and the inductive bias provided by symplectic invariants.

### C.1. Overall Map

The full transformation is

$$(\mathbf{q}_t, \mathbf{p}_t) \mapsto \mathbf{z}_c = \Phi_{\theta_{SE}}(\mathbf{q}_t, \mathbf{p}_t) \mapsto \mathbf{z}_d = \Phi_{\theta_{AD}}(\mathbf{z}_c, \mathbf{u}_t, \mathbf{d}_t).$$

Hence, at the *global* level, we define

$$\Phi_{\theta}(\mathbf{q}_t, \mathbf{p}_t, \mathbf{u}_t, \mathbf{d}_t) := \Phi_{\theta_{AD}}(\Phi_{\theta_{SE}}(\mathbf{q}_t, \mathbf{p}_t), \mathbf{u}_t, \mathbf{d}_t).$$

We aim to show that if  $\Phi_{\theta_{AD}}$  remains a *small* (bounded) perturbation from identity in  $\mathbf{z}_c$ -space, then  $\Phi_{\theta}$  preserves the symplectic structure up to a small error term. This is called *near-symplecticity*. We assume that the dissipation  $\mathbf{d}_t$  is seperable for the sake of this proof.

### C.2. SymplecticEncoder

From Jin *et al.*, we know that *LA-SympNets* are fully symplectic due to their construction (Jin *et al.*, 2020). By extension, we can show that our SymplecticEncoder  $\Phi_{\theta_{SE}}$ .

**Definition C.1** (Symplectic Property). Let  $\mathcal{X} = \mathbb{R}^{2d}$  represent the canonical phase space with coordinates  $\mathbf{x} \in (\mathbf{q}, \mathbf{p})$ . We write

$$J = \begin{pmatrix} 0 & I_d \\ -I_d & 0 \end{pmatrix},$$

the standard  $2d \times 2d$  symplectic matrix. A differentiable map  $\Psi : \mathcal{X} \rightarrow \mathcal{X}$  is *strictly symplectic* if

$$d\Psi(\mathbf{x})^\top J d\Psi(\mathbf{x}) = J \quad \forall \mathbf{x} \in \mathcal{X}.$$

This implies  $\det(d\Psi) = 1$  (volume preservation).

We know

$$\Phi_{\theta_{SE}} : \mathcal{X} \rightarrow \mathcal{Z} \subseteq \mathbb{R}^{2d}$$

is strictly symplectic, i.e.

$$d\Phi_{\theta_{SE}}(\mathbf{x})^\top J d\Phi_{\theta_{SE}}(\mathbf{x}) = J, \quad \det(d\Phi_{\theta_{SE}}(\mathbf{x})) = 1.$$

Internally, since  $\Phi_{\theta_{SE}}$  is a composition of symplectic sub-blocks (e.g. LA-SympNets). Its parameters,  $\theta_{SE}$ , can be partially meta-learned as long as the strict symplectic property is retained.

### C.3. Decoder with Control and Dissipation

We define

$$\Phi_{\theta_{AD}} : \mathcal{Z} \times \mathcal{U} \times \mathcal{D} \rightarrow \mathcal{Z},$$

where:

- $\mathcal{Z} \subseteq \mathbb{R}^{2d}$  is the latent phase-space output by  $\Phi_{\theta_{SE}}$ ,
- $\mathcal{U} \subseteq \mathbb{R}^m$  represents *control signals* (bounded by  $\|\mathbf{u}_t\| \leq U_{\max}$ ),
- $\mathcal{D} \subseteq \mathbb{R}^r$  represents *dissipative parameters* (bounded by  $\|\mathbf{d}_t\| \leq D_{\max}$ ), which model forces that remove or drain energy (e.g. friction or drag).

The decoder modifies the latent state by

$$\Phi_{\theta_{AD}}(\mathbf{z}_c, \mathbf{u}_t, \mathbf{d}_t) = \mathbf{z}_c + F_{\theta_{AD}}(\mathbf{z}_c, \mathbf{u}_t, \mathbf{d}_t),$$

where  $F_{\theta_{AD}}$  can be cross-attention with magnitude modulated by  $\|\mathbf{u}_t\|$ , or a damping formula modulated by  $\|\mathbf{d}_t\|$ .

#### C.4. Near-Symplectic Proof and Explicit Bound

In this section, we want to prove that if  $\mathbf{z}_c \mapsto \mathbf{z}_c + F_{\theta_{AD}}(\mathbf{z}_c)$  is a *bounded perturbation* from identity (in partial derivatives), then the composition with a strict symplectic map remains close to preserving  $J$ .

**Bounded Perturbation Assumption.** For the ActiveDecoder map, we assume the partial derivative w.r.t.  $\mathbf{z}_c$  in  $F_{\theta_{AD}}$  is *bounded* by a linear-type function of  $(\|\mathbf{u}_t\|, \|\mathbf{d}_t\|)$ :

$$\left\| \frac{\partial F_{\theta_{AD}}}{\partial \mathbf{z}_c}(\mathbf{z}_c, \mathbf{u}_t, \mathbf{d}_t) \right\| \leq \alpha_0 + \alpha_u \|\mathbf{u}_t\| + \alpha_d \|\mathbf{d}_t\|,$$

for some constants  $\alpha_0, \alpha_u, \alpha_d \geq 0$ . This covers *cross-attention* (scaled by  $\|\mathbf{u}_t\|$ ) and *dissipative* (scaled by  $\|\mathbf{d}_t\|$ ) terms. Since  $\|\mathbf{u}_t\| \leq U_{\max}$  and  $\|\mathbf{d}_t\| \leq D_{\max}$ , we define:

$$\rho := \alpha_0 + \alpha_u U_{\max} + \alpha_d D_{\max}.$$

Hence,  $\max_{(\mathbf{z}_c, \mathbf{u}_t, \mathbf{d}_t)} \|\mathbf{d}_{\mathbf{z}_c} \Phi_{\theta_{AD}} - I\| \leq \rho$ . Equivalently,

$$\left\| \mathbf{d}_{\mathbf{z}_c} F_{\theta_{AD}}(\mathbf{z}_c, \mathbf{u}_t, \mathbf{d}_t) \right\| \leq \rho, \quad \forall (\mathbf{z}_c, \mathbf{u}_t, \mathbf{d}_t).$$

**The Composed Map.** Recall we define the global map

$$\Phi_{\theta}(\mathbf{q}_t, \mathbf{p}_t, \mathbf{u}_t, \mathbf{d}_t) = \Phi_{\theta_{AD}}\left(\Phi_{\theta_{SE}}(\mathbf{q}_t, \mathbf{p}_t), \mathbf{u}_t, \mathbf{d}_t\right).$$

Writing  $\mathbf{x} = (\mathbf{q}_t, \mathbf{p}_t) \in \mathbb{R}^{2d}$  for convenience, we have

$$\mathbf{z}_c = \Phi_{\theta_{SE}}(\mathbf{x}) \quad \text{and} \quad \mathbf{z}_d = \Phi_{\theta_{AD}}(\mathbf{z}_c, \mathbf{u}_t, \mathbf{d}_t).$$

To show near-symplecticity, we study

$$\mathbf{d}\Phi_{\theta}(\mathbf{x}, \mathbf{u}_t, \mathbf{d}_t) = \underbrace{\mathbf{d}_{\mathbf{z}_c} \Phi_{\theta_{AD}}(\mathbf{z}_c, \mathbf{u}_t, \mathbf{d}_t)}_{I + A, \|A\| \leq \rho} \times \underbrace{\mathbf{d}\Phi_{\theta_{SE}}(\mathbf{x})}_{\text{strictly symplectic}}.$$

**Theorem C.2 (Near-Symplectic Composition).** *Suppose  $\Phi_{\theta_{SE}}$  is strictly symplectic, i.e.*

$$\mathbf{d}\Phi_{\theta_{SE}}(\mathbf{x})^{\top} J \mathbf{d}\Phi_{\theta_{SE}}(\mathbf{x}) = J \quad \text{and} \quad \det(\mathbf{d}\Phi_{\theta_{SE}}(\mathbf{x})) = 1.$$

*Also assume  $\mathbf{d}_{\mathbf{z}_c} \Phi_{\theta_{AD}}$  satisfies the bounded-perturbation condition  $\max \|\mathbf{d}_{\mathbf{z}_c} \Phi_{\theta_{AD}} - I\| \leq \rho$  over  $\|\mathbf{u}_t\| \leq U_{\max}$ ,  $\|\mathbf{d}_t\| \leq D_{\max}$ . Then for the composed map  $\Phi_{\theta}$ , we have:*

$$\left\| \mathbf{d}\Phi_{\theta}(\mathbf{x})^{\top} J \mathbf{d}\Phi_{\theta}(\mathbf{x}) - J \right\| \leq C \rho,$$

*for a constant  $C > 0$  depending on the norm of  $\mathbf{d}\Phi_{\theta_{SE}}(\mathbf{x})$ . Hence  $\Phi_{\theta}$  is  $\epsilon$ -symplectic with  $\epsilon = C \rho$ . Furthermore,*

$$\det(\mathbf{d}\Phi_{\theta}(\mathbf{x})) = \mathbf{1} + O(\rho),$$

*implying near-volume preservation as well.*

*Sketch of Proof.* Let  $\mathbf{x} = (\mathbf{q}_t, \mathbf{p}_t)$ ,  $\mathbf{z}_c = \Phi_{\theta_{SE}}(\mathbf{x})$ , and  $I + A = d_{\mathbf{z}_c} \Phi_{\theta_{AD}}(\mathbf{z}_c, \mathbf{u}_t, \mathbf{d}_t)$  with  $\|A\| \leq \rho$ . Then

$$d\Phi_{\theta}(\mathbf{x}, \mathbf{u}_t, \mathbf{d}_t) = (I + A) d\Phi_{\theta_{SE}}(\mathbf{x}).$$

Hence

$$d\Phi_{\theta}^{\top} J d\Phi_{\theta} = d\Phi_{\theta_{SE}}^{\top} (I + A)^{\top} J (I + A) d\Phi_{\theta_{SE}}.$$

Expanding  $(I + A)^{\top} J (I + A) = J + A^{\top} J + J A + A^{\top} J A = J + O(\|A\|)$ , we substitute  $d\Phi_{\theta_{SE}}^{\top} J d\Phi_{\theta_{SE}} = J$ :

$$d\Phi_{\theta}^{\top} J d\Phi_{\theta} = J + O(\|A\|) = J + O(\rho).$$

In operator norm,  $\|d\Phi_{\theta}^{\top} J d\Phi_{\theta} - J\| \leq C \rho$ . Since  $d\Phi_{\theta_{SE}}$  is volume-preserving,  $\det(d\Phi_{\theta}) = \det(I + A) \times \mathbf{1} = \mathbf{1} + O(\rho)$ .  $\square$

**Explicit Cross-Attention Bound.** For instance, if  $F_{\theta_{AD}}$  includes a *cross-attention* term scaled by  $\|\mathbf{u}_t\|$  plus a *dissipative* term scaled by  $\|\mathbf{d}_t\|$ , we might write

$$F_{\theta_{AD}}(\mathbf{z}_c, \mathbf{u}_t, \mathbf{d}_t) = \alpha \text{CrossAttn}(\mathbf{z}_c, \mathbf{u}_t) - \gamma (\mathbf{d}_t^{\top} \star \mathbf{z}_c),$$

where  $\mathbf{d}_t^{\top} \star \mathbf{z}_c$  indicates some parametric dissipator. If  $\text{CrossAttn}$  has partial derivative in  $\mathbf{z}_c$  normed by  $\|\mathbf{u}_t\|$ , and  $\mathbf{d}_t^{\top} \star \mathbf{z}_c$  is linear in  $\|\mathbf{d}_t\|$ , then

$$\left\| \frac{\partial F_{\theta_{AD}}}{\partial \mathbf{z}_c} \right\| \leq \alpha_0 + \alpha_u \|\mathbf{u}_t\| + \alpha_d \|\mathbf{d}_t\|,$$

giving the same  $\rho = \alpha_0 + \alpha_u U_{\max} + \alpha_d D_{\max}$ . Provided  $\rho \ll 1$ ,  $\Phi_{\theta}$  remains near-symplectic.